

Supporting Information

Initiator loaded separator triggering in-situ polymerization of poly(1,3-dioxolane) quasi-solid electrolyte for lithium metal batteries

Hao Huang^{a,b}, Chaohui Wei^b, Qiang Zhao^{a,b}, Aijun Zhou^{a,b}, Jingze Li^{a,b*}

a School of Materials and Energy, University of Electronic Science and Technology of China, Chengdu 611731, P. R. China

b Huzhou Key Laboratory of Smart and Clean Energy, Yangtze Delta Region Institute (Huzhou), University of Electronic Science and Technology of China, Huzhou 313001, P. R. China

Corresponding author E-mail: lijingze@uestc.edu.cn (J. Z. Li)

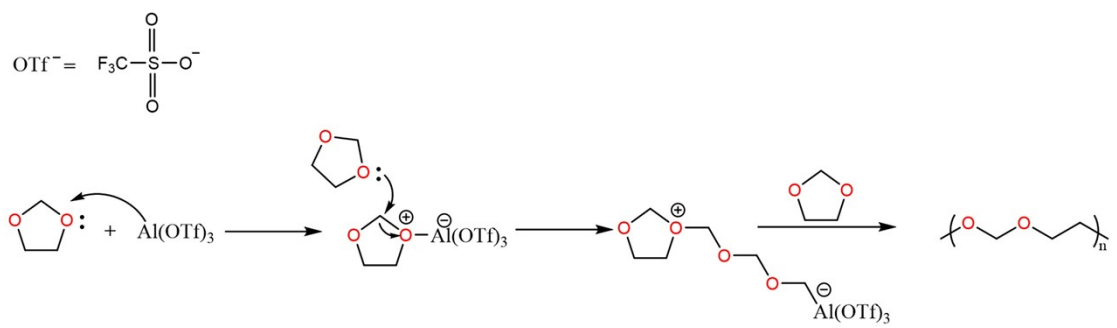


Fig. S1. Illustration of the reaction mechanism of DOL in situ polymerization.

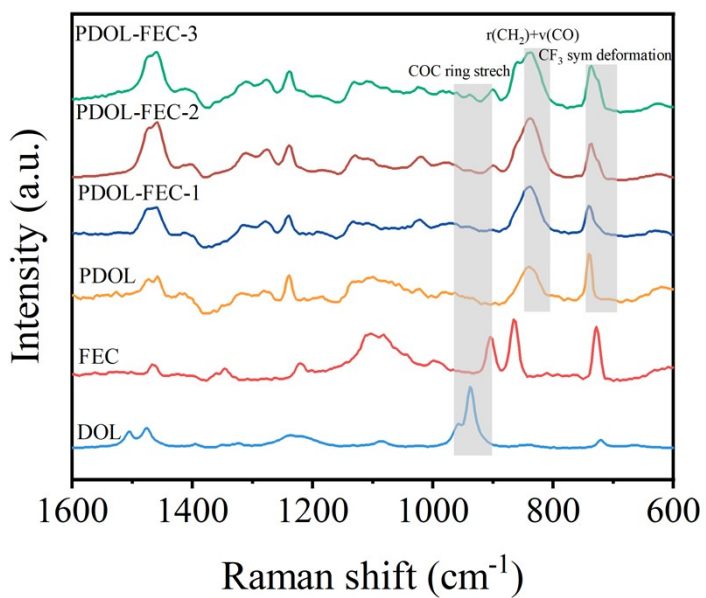


Fig. S2 Raman spectra of different electrolytes.

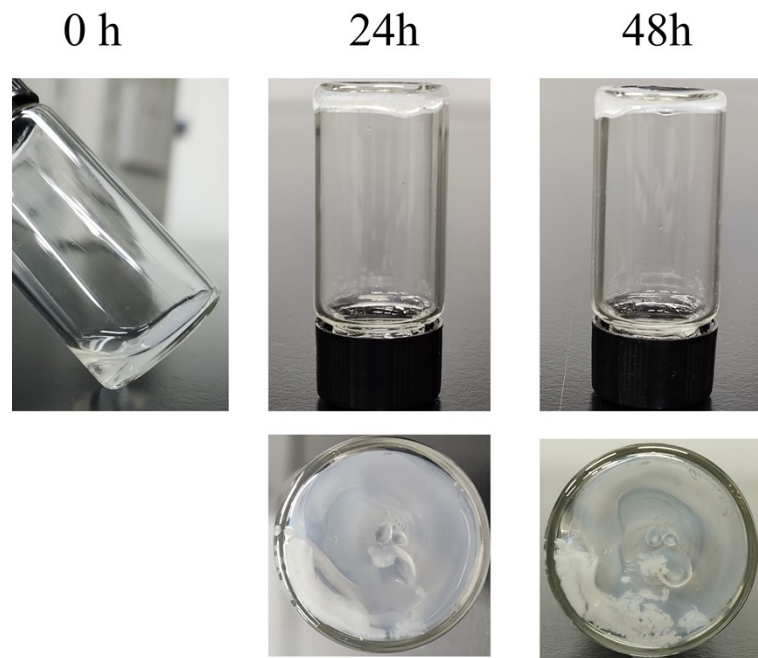


Fig. S3 Digital images of DOL precursor in the bottle before and after $\text{Al}(\text{OTf})_3$ loaded separator initiated polymerization for 24 and 48h.

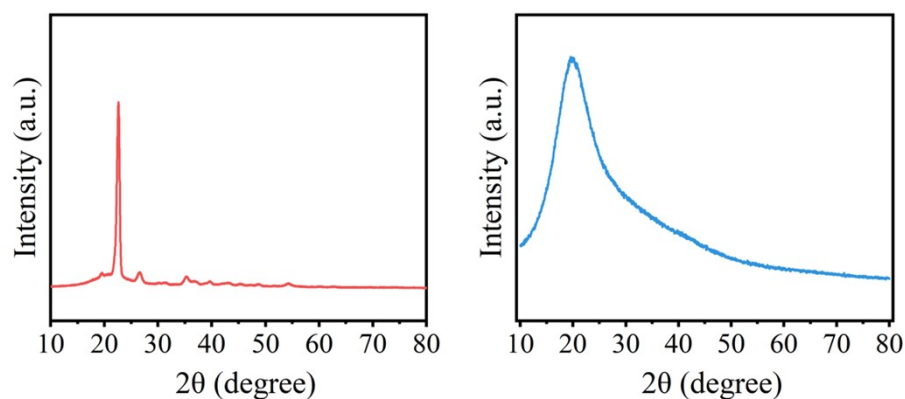


Fig. S4 XRD patterns of different parts of the GPE. (a) near the separator and (b) away from the separator.

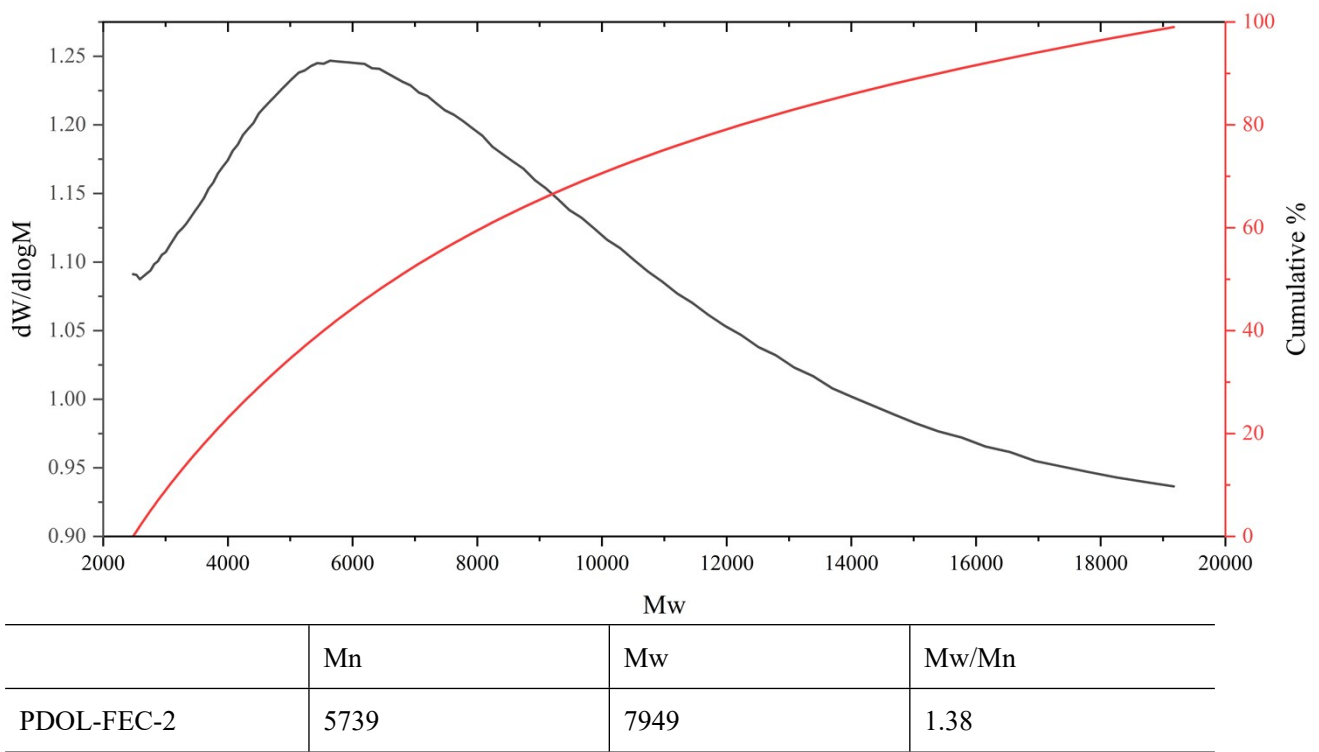


Fig. S5. GPC data of PDOL-FEC-2 with THF as the solvent.

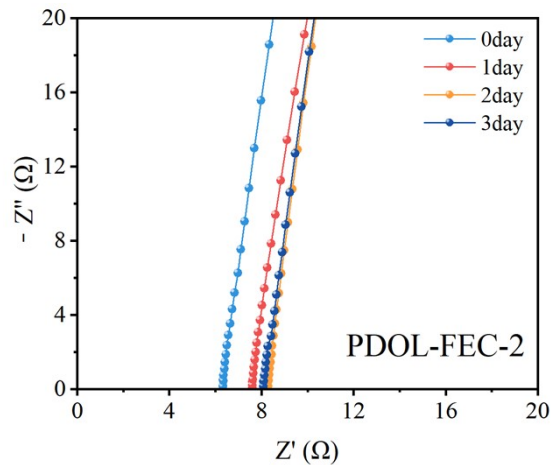


Fig. S6. EIS spectra of SS|PDOL-FEC-2|SS cell at room temperature as a function of the storage time.

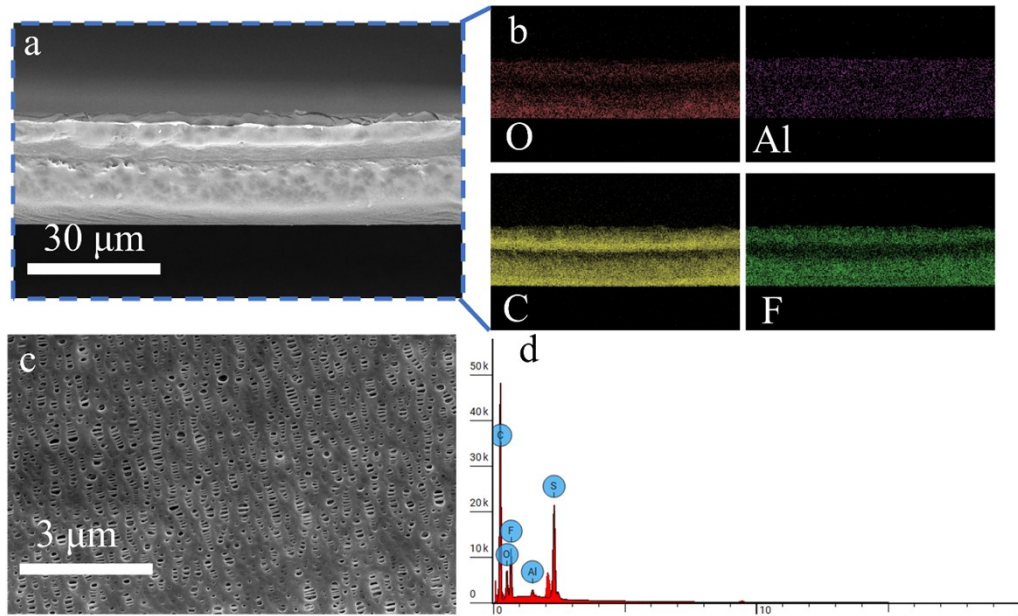


Fig. S7 (a) Cross-section SEM image of the Al (OTf)₃-loaded separator. (b) Cross-section EDS mapping images of the cross-section of the Al (OTf)₃-loaded separator. (c) Top-view SEM image of the PP separator. (d) EDS curve of the composite separator.

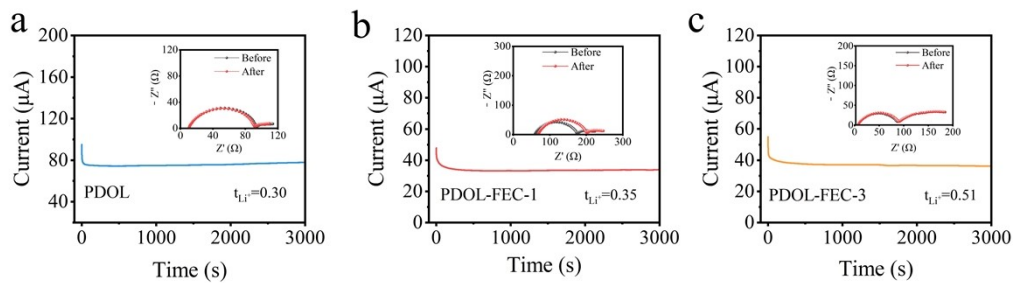


Fig. S8 chronoamperometry curves with a step voltage of 10 mV of cells with (a)PDOL, (b)PDOL-FEC-1, and (c)PDOL-FEC-3.The insets displayed EIS plots before and after polarization.

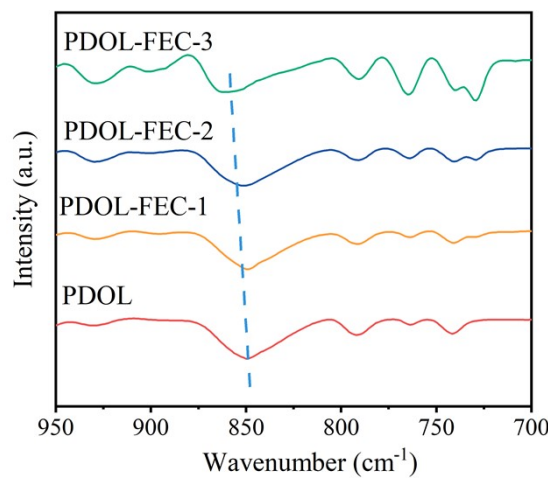


Fig. S9. FTIR spectra of PDOL, PDOL-FEC-1, PDOL-FEC-2, and PDOL-FEC-3.

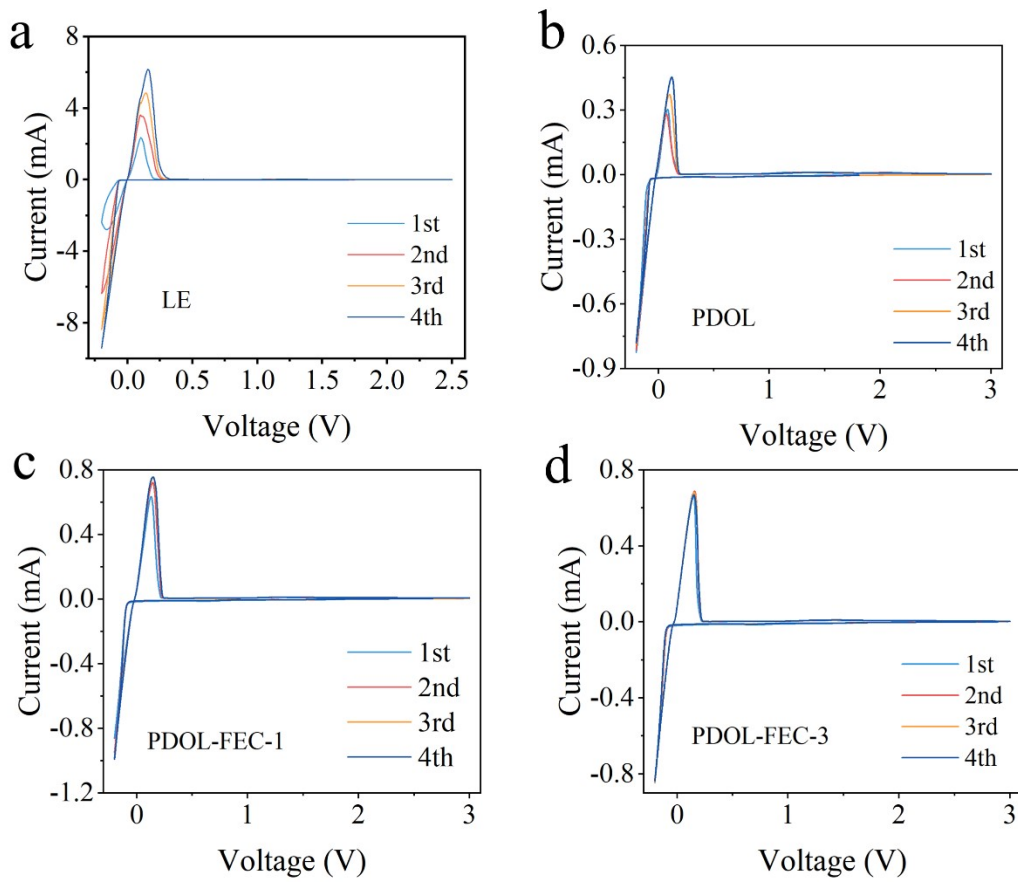


Fig. S10. CV curves of the Li|SS cells with (a)LE, (b)PDOL, (c)PDOL-FEC-1, and (d)PDOL-FEC-3.

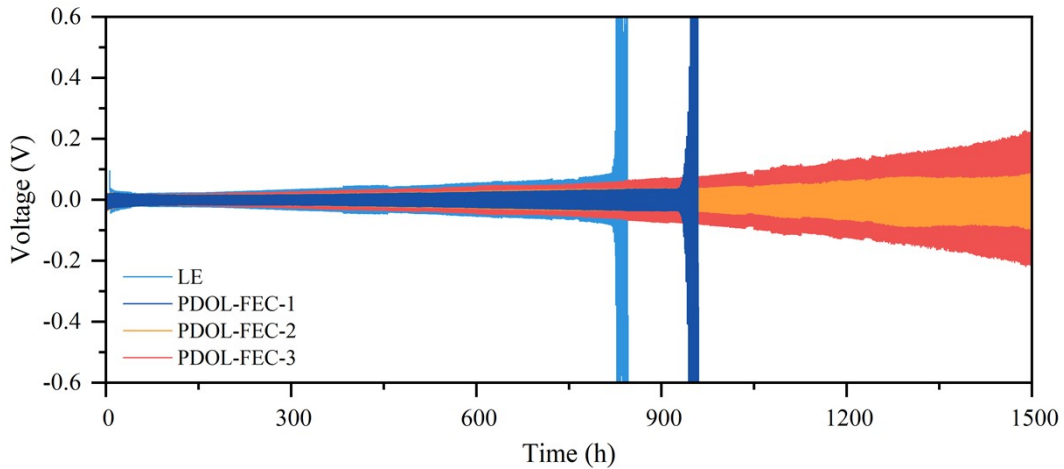


Fig. S11. Voltage profiles of Li//Li symmetrical cells that contain different electrolytes at room temperature with the current density of 0.5 mAh cm^{-2} .

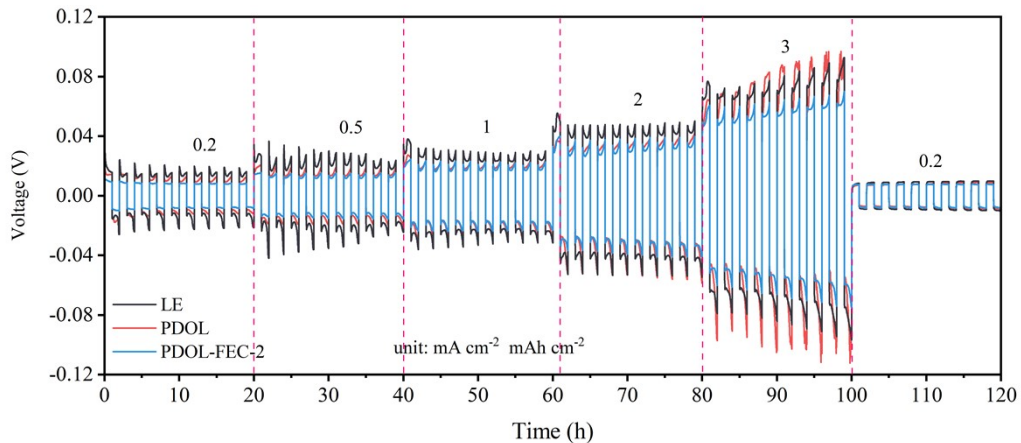


Fig. S12. Voltage profiles of Li||Li cells at different current densities.

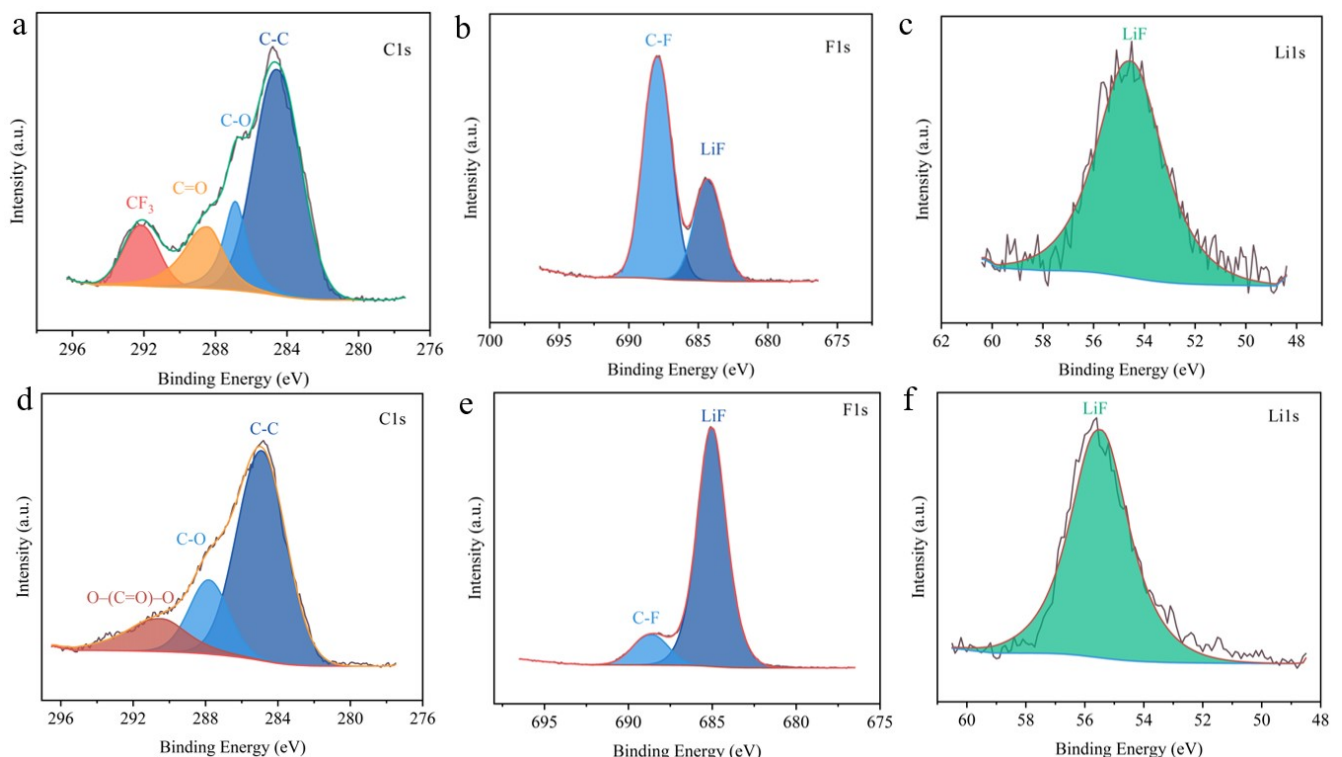


Fig S13 XPS spectra (C 1s, F 1s and Li 1s spectra) of the Li metal surface from the cycled Li||Li cells after 50 h at 1 mA cm^{-2} for 1 mA h cm^{-2} : (a , b and c) LE cell and (d, e and f) GPE cell (PDOL-FEC-2)

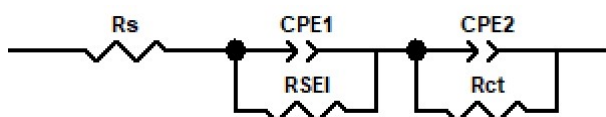


Fig. S14 Equivalent circuit for fitting Nyquist plots of Li||Li symmetric cells.

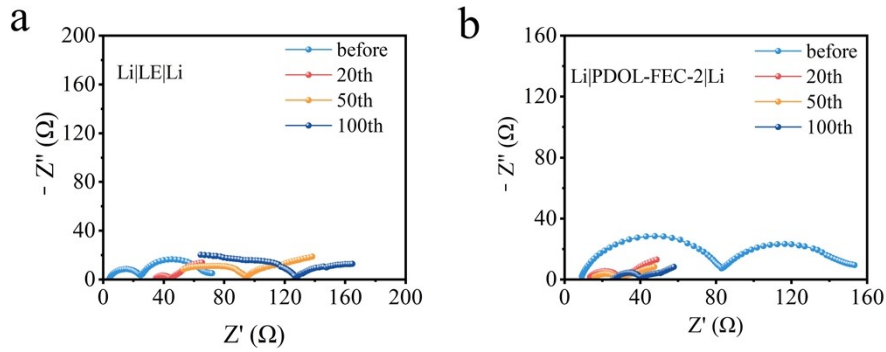


Fig. S15. The EIS of Li/Li cells with the LE (a) and (b) PDOL-FEC-2.

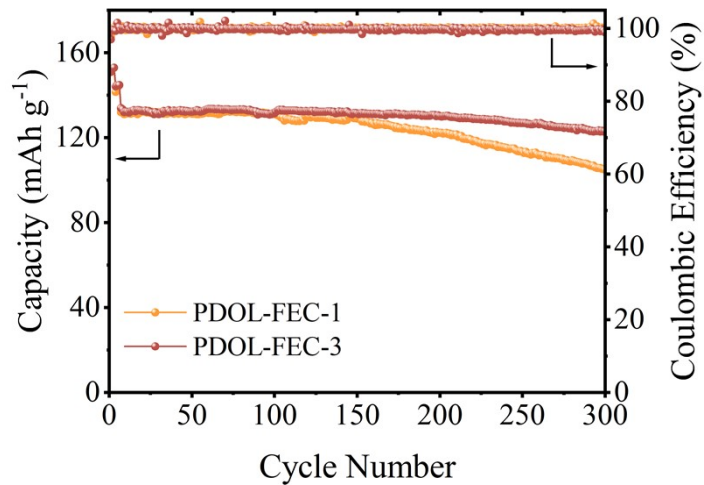


Fig. S16. Cycling performances and CE of the $\text{LFP}||\text{Li}$ cell at room temperature with PDOL-FEC-1 and PDOL-FEC-3 electrolytes at 1 C.

Table S1 Liquid content of different electrolytes

| Sample | liquid content. |
|------------|-----------------|
| PDOL | 2.2% |
| PDOL-FEC-1 | 4.5% |
| PDOL-FEC-2 | 9.2% |
| PDOL-FEC-3 | 10.2% |

Table S2 The fitted EIS parameters of $\text{Li}|\text{LE}|\text{Li}$ and $\text{Li}|\text{PDOL-FEC-2}|\text{Li}$ batteries

| | | R_s | R_{SEI} | R_{ct} |
|---------------------------------|--------|-------|-----------|----------|
| $\text{Li} \text{LE} \text{Li}$ | Before | 4.238 | 19.72 | 46.35 |
| | 20th | 9.911 | 6.362 | 4.229 |

| | | | | |
|------------------|--------|-------|-------|-------|
| | 50th | 13.81 | 8.716 | 5.186 |
| | 100th | 28.47 | 12.36 | 6.782 |
| Li PDOL-FEC-2 Li | Before | 8.459 | 75.08 | 61.84 |
| | 20th | 12.63 | 16.66 | 16.25 |
| | 50th | 16.14 | 11.55 | 16.75 |
| | 100th | 27.41 | 12.53 | 17.71 |
| | | | | |

Table S3 Comparison of our work with previously reported PDOL-based electrolytes via in-situ polymerization

| Electrolyte | Initiator | Ionic Conductivity, t_{Li}^+ | Li//Li cell performance | Battery performance | Ref |
|-------------------------------|--|---|--|---|--------------|
| 2 M LiTFSI +DOL | 0.5mM Al (OTf) ₃ | 1×10^{-3} S cm ⁻¹ | 400 h; 1.0 mA cm ⁻² , 1.0 mAh cm ⁻² | 1 C, 700 cycles | ¹ |
| DOL+DME +1M LiTFSI | 2M LiPF ₆ | 5.50×10^{-4} S cm ⁻¹ | 400 h; 1.0 mA cm ⁻² , 1.0 mAh cm ⁻² | 0.5 C, 700 cycles, capacity retention:95.6% | ² |
| DOL/FEC (v/v=10:1) +2M LiTFSI | 0.43mM Al(OTf) ₃ | 2.4×10^{-5} S cm ⁻¹ at - 60 °C; 0.55 at -20°C | 850 h; 0.2 mA cm ⁻² , 0.2 mAh cm ⁻² at 0°C | 0.2 C, 400 cycles, capacity retention:96% at 0 °C | ³ |
| 2 M LiTFSI +DOL | Sc(OTf) ₃ | 1.07×10^{-3} S cm ⁻¹ | / | 1 C, 200 cycles, capacity retention:92.3% | ⁴ |
| 2 M LiTFSI +DOL | 0.4mM Al (OTf) ₃ | 2.39×10^{-3} S cm ⁻¹ | 250 h; 0.5 mA cm ⁻² , 1.0 mAh cm ⁻² | 1 C, 200 cycles, capacity retention:69.96% | ⁵ |
| DOL+DME+1M LiTFSI | acid-treated nano Al ₂ O ₃ | 3.37×10^{-3} S cm ⁻¹ ; 0.74 | 1000 h; 1.0 mA cm ⁻² , 1.0 mAh cm ⁻² | 200cycles, capacity retention:82.1% | ⁶ |
| DOL+SCN+FEC +1 M LiTFSI | 0.4 M LiBF ₄ | 1.95×10^{-4} S cm ⁻¹ ; 0.36 | 600 h; 0.2 mA cm ⁻² , 0.2 mAh cm ⁻² | 0.5C,1000 cycles, capacity retention:80% | ⁷ |
| DOL/FEC (v/v=10:2) +1M LiTFSI | Al (OTf) ₃ | 1.5×10^{-4} S cm ⁻¹ ; 0.63 | 650 h; 1.0 mA cm ⁻² , 1.0 mAh cm ⁻² | 1C, 300 cycles, capacity retention:94.5% | This work |

- Q. Zhao, X. T. Liu, S. Stalin, K. Khan and L. A. Archer, *Nature Energy*, 2019, **4**, 365-373.
- F. Q. Liu, W. P. Wang, Y. X. Yin, S. F. Zhang, J. L. Shi, L. Wang, X. D. Zhang, Y. Zheng, J. J. Zhou,

- L. Li and Y. G. Guo, *Science Advances*, 2018, **4**, eaat5383.
- 3. W. Ren, Y. Zhang, R. Lv, S. Guo, W. Wu, Y. Liu and J. Wang, *Journal of Power Sources*, 2022, **542**, 231773.
 - 4. G. Yang, Y. Zhai, J. Yao, S. Song, L. Lin, W. Tang, Z. Wen, N. Hu and L. J. C. C. Lu, *Chemical Communications*, 2021, **57**, 7934-7937.
 - 5. D. Chen, M. Zhu, P. Kang, T. Zhu, H. Yuan, J. Lan, X. Yang and G. J. A. S. Sui, *Advanced Science* 2022, **9**, 2103663.
 - 6. S. Wang, L. Zhou, M. K. Tufail, L. Yang, P. Zhai, R. Chen and W. J. C. E. J. Yang, 2021, **415**, 128846.
 - 7. Y. Bai, W. Ma, W. Dong, Y. Wu, X. Wang and F. Huang, *ACS Appl Mater Interfaces*, 2023, **15**, 26834-26842.